

Special  
Collection

# Initial Stages of Sodium Deposition onto Au(111) from [MPPip][TFSI]: An In-Situ STM Study for Sodium-Ion Battery Electrolytes

Maren-Kathrin Heubach,<sup>[a]</sup> Fabian M. Schuett,<sup>[a]</sup> Ludwig A. Kibler,<sup>[a]</sup> Areeg Abdelrahman,<sup>\*,[a]</sup> and Timo Jacob<sup>\*,[a, b, c]</sup>

Sodium-ion batteries are promising candidates for post-lithium-ion batteries. While sodium has a less negative standard electrode potential compared to lithium, it is still a strong reducing agent. Ionic liquids are suitable solvents for sodium metal batteries, since metallic sodium is very reactive, particularly with water and molecules containing acidic hydrogen atoms. In this study, the initial stages of electrodeposition of sodium on Au(111) from *N*-methyl-*N*-propylpiperidinium [MPPip] bis(trifluoromethanesulfonyl)imide [TFSI] were studied

using voltammetry and in-situ scanning tunnelling microscopy. Four subsequent underpotential deposition stages were observed: (i) nucleation at the Au(111) reconstruction elbows, followed by (ii) growth of small monoatomically high islands that form (iii) a smooth layer via coalescence, and (iv) further island growth on top of the existing layers. The electrocrystallisation mode changed from smooth layer formation to 3D growth, resulting in cauliflower-like structures. The deposition process was accompanied by simultaneous alloy formation.

## Introduction

The demand for energy storage systems has significantly increased in recent years due to the increasing amount of renewable energy sources and the growing number of portable devices in everyday use.<sup>[1–4]</sup> Lithium and cobalt, which are typically used in lithium-ion batteries are scarce, hence other metals such as sodium are now being explored. The natural abundance of sodium as well as the fact that, unlike lithium, it is inert toward nitrogen and aluminium, are two of its major advantages.<sup>[5]</sup> Sodium is reactive and requires specific electrolytes due to its low reduction potential (2.71 V vs. SHE).<sup>[6]</sup> Nevertheless, sodium-based battery research has been limited in recent years due to several drawbacks. Dendritic growth is one of the major problems since it can lead to internal short-circuits and thus to a thermal runaway, which is extremely

dangerous.<sup>[7–9]</sup> Chemical reactions with standard battery electrolytes such as organic carbonates,<sup>[10]</sup> which are commonly used in lithium-ion batteries,<sup>[11]</sup> pose another concern.


Metallic sodium is very reactive, especially with water, acidic hydrogen-containing molecules, and organic carbonates.<sup>[10]</sup> Room temperature ionic liquids (RTILs), often referred to as ionic liquids (ILs), have a wider electrochemical window and a lower electrochemical resistance compared to most organic solvents, and are thus promising solvents for sodium salts in sodium metal batteries.<sup>[12]</sup> The fact that they are salts, and therefore composed of charged species, allows them to have these properties.<sup>[13]</sup> They crystallise at temperatures below room temperature due to their large organic cations and may therefore be used as electrolytes and solvents in various applications.<sup>[14]</sup> The wide electrochemical stability windows enable the plating and stripping of metals such as lithium and sodium without degradation of the electrolyte.<sup>[6]</sup> *N*-butyl-*N*-methylpyrrolidinium bis(trifluoromethanesulfonyl)imide ([C<sub>4</sub>mpyr][TFSI]), in particular, was observed to be a suitable electrolyte for sodium plating and dissolution.<sup>[6,9,15]</sup> Still, ionic liquids exhibit relatively high viscosities and thus rather low diffusion rates.<sup>[13]</sup> While this is a drawback for most applications, it is ideal for real-time investigations since the processes are slower and easier to follow. In the present study, an electrolyte based on *N*-methyl-*N*-propylpiperidinium bis(trifluoromethanesulfonyl)imide ([MPPip][TFSI]) is used. This ionic liquid has previously been used in interfacial studies<sup>[16]</sup> and for the investigation of lithium and zinc electrodeposition onto gold single crystal model surfaces.<sup>[17,18]</sup>

In-situ microscopic imaging of metal deposition processes and electrodeposits helps revealing topographical changes of the surface on an atomic level in real space, which can then be compared to results obtained with macroscopic electrochemical techniques. Significant progress has been made in studying the


[a] M.-K. Heubach, F. M. Schuett, Dr. L. A. Kibler, Dr. A. Abdelrahman, Prof. Dr. T. Jacob  
Institute of Electrochemistry, Ulm University  
Albert-Einstein-Allee 47, 89081 Ulm, Germany  
E-mail: areeg.abdelrahman@alumni.uni-ulm.de  
timo.jacob@uni-ulm.de

[b] Prof. Dr. T. Jacob  
Helmholtz-Institute-Ulm (HIU)  
Electrochemical Energy Storage  
Helmholtzstr. 11, 89081 Ulm, Germany

[c] Prof. Dr. T. Jacob  
Karlsruhe Institute of Technology (KIT)  
P.O. Box 3640, 76021 Karlsruhe, Germany

 Supporting information for this article is available on the WWW under <https://doi.org/10.1002/celec.202200722>

 An invited contribution to the Retiring Board Members Special Collection.

 © 2022 The Authors. ChemElectroChem published by Wiley-VCH GmbH. This is an open access article under the terms of the Creative Commons Attribution Non-Commercial NoDerivs License, which permits use and distribution in any medium, provided the original work is properly cited, the use is non-commercial and no modifications or adaptations are made.

deposition and stripping behaviour of metals on electrode surfaces on an atomic scale using in-situ scanning tunnelling microscopy (STM). To investigate the metal deposition processes, especially underpotential deposition (UPD) at a fundamental level, well-ordered model systems, specifically single-crystal electrode surfaces, have been well-established.<sup>[19–21]</sup> Observing initial microscopic stages is key to understanding the macroscopic morphology of the deposit. In some cases, the initial stages already show processes as early as dendrite formation.<sup>[17]</sup> Despite this, studies focusing on the initial stages of metal deposition are still scarce.

Gold single crystals are commonly used in in-situ STM studies due to their (i) well-defined surface structure, (ii) ease in preparation, and (iii) noble character in terms of their stability towards water and oxygen.<sup>[22]</sup> Among the different single crystal surfaces of Au, the densely packed (111) orientation is the most investigated in fundamental studies of the initial stages of metal deposition.<sup>[17,18,23–25]</sup> It has been reported that the deposition of lithium on Au(111) starts at underpotential shifts of more than 1 V,<sup>[23]</sup> where the first islands are deposited.<sup>[17,23]</sup> At underpotentials, subsequent layer growth covers two or more layers.<sup>[23]</sup> This is in contrast to simpler systems such as copper or silver UPD on Au(111) which cover only one or two monolayers, respectively.<sup>[26,27]</sup> The bulk deposition occurs in a three-dimensional growth mode.<sup>[17]</sup> The deposition of lithium appears to be coupled with the formation of an alloy with the gold substrate.<sup>[17,23]</sup>

In the case of sodium deposition onto Au, alloy formation is expected since there are three different stable bulk alloys: Au<sub>2</sub>Na, AuNa, and AuNa<sub>2</sub>.<sup>[28]</sup> According to electrochemical and UHV studies, gold, which is known to be sodiophilic, spontaneously forms alloys when in contact with sodium.<sup>[29,30]</sup> Additionally, sodium has been reported to have excellent deposition behaviour on a sodium-gold alloy that has already been formed.<sup>[31]</sup>

The majority of published research on sodium deposition from ionic liquids focuses on the overall stability of the system or the nature of the electrolyte.<sup>[6,9,15]</sup> However, there are very few studies on the initial stages of sodium deposition.<sup>[32,33]</sup> To our knowledge, none of these studies resolves the initial stages on the nanoscale. A fundamental understanding of the electrochemical behaviour of similar systems using single-crystal electrodes is of utmost importance to aid in the development and design of sodium-ion batteries. Therefore, this study aims to use voltammetry and in-situ STM to observe and attempt to understand the initial stages of sodium deposition and the observation of four subsequent stages in the deposition mechanism. The findings are later compared with those of lithium deposition under similar electrochemical conditions.<sup>[17,23,24]</sup>

## Results and Discussion

### Electrochemical behaviour

#### Pure ionic liquid

It is necessary to first investigate the behaviour of the pure ionic liquid to distinguish the processes induced by sodium from those involving the pure ionic liquid. Figure 1 shows a positive-going (blue curve) and a negative-going linear potential sweep (red curve) for Au(111) in [MPPip][TFSI] at 5 mVs<sup>-1</sup>. The electrochemical stability window of the ionic liquid in contact with the Au(111) electrode is around 5 V, between the cathodic and the anodic processes at C4' and A3', with onset potentials at -0.18 V and 4.92 V, respectively. It should, however, be noticed that the system's stability is limited by cathodic and anodic corrosion of the Au(111) electrode at C3' and A2' with onset potentials around 0.28 V and 4.25 V, respectively.

Both cathodic and anodic corrosion processes at the Au(111) electrode surface are observed by in-situ STM measurements. Cathodic corrosion begins at 0.8 V (Figure S1a) by pit formation while anodic corrosion begins at potentials positive of 3.8 V by gold dissolution. (Figure S1b). Further increase of the potential to 4.9 V results in drastic anodic corrosion, leading to bad STM image quality. After decreasing the potential again to values where the surface is stable, the surface exhibits many monoatomically deep holes and is thus much rougher than before. There are no signs of ionic liquid decomposition at these potentials, which includes the formation of 5–50 nm high clusters of undefined shape and the electrode surface losing its conductive properties resulting in poor imaging quality. The difference between the electrochemical stability window in the potential sweep experiments and the in-situ STM measurement can be explained by differences in the water content. An

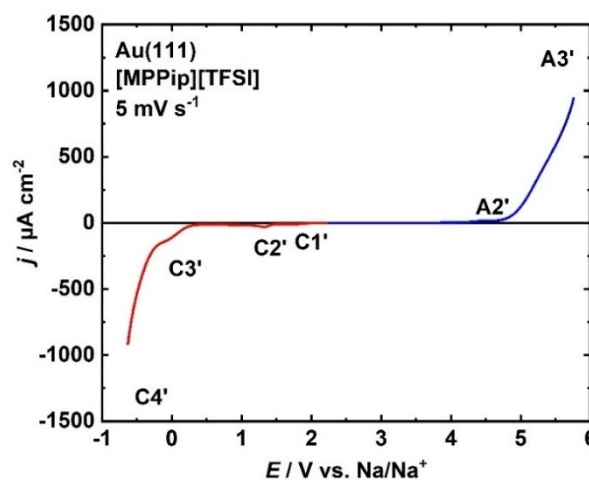


**Figure 1.** Negative-going (red curve) and positive-going (blue curve) linear potential sweep curves of Au(111) in [MPPip][TFSI]. The Faraday processes C4' and A3' indicate the electrochemical stability window of the ionic liquid. The peaks C3' and A2' are associated with cathodic and anodic corrosion of gold, respectively. C1' and C2' are attributed to residual water.

increased water content results in an increased concentration of hydroxide anions which significantly influences cathodic corrosion.<sup>[34]</sup> Preliminary measurements have shown that the onset potential of the cathodic corrosion can shift by 0.6 V if the water content is increased from 20 to 200 ppm. The features C2' and C1' are most likely related to processes that involve residual water and have a counter feature A1' at 2.7 V, which appears after C1' and C2' were previously swept. As a result, it is not observed in the voltammetric curve depicted in Figure 1. Summarising, the cathodic corrosion of the Au(111) electrode is positive of the Na/Na<sup>+</sup> equilibrium potential. For a well-ordered Au(111) electrode surface, sodium underpotential deposition (UPD) is observed to start at a potential positive of the onset potential of cathodic corrosion. A similarly high underpotential shift has already been reported for sodium deposition on nickel,<sup>[6]</sup> as well as for lithium deposition on Au(111).<sup>[17,23,24]</sup>

### Sodium-containing electrolyte

Figure 2 shows current-potential curves of Au(111) in [MPPip][TFSI] + 0.2 M Na[TFSI] at 5 mV s<sup>-1</sup> with different negative potential limits. All curves were recorded subsequently in a single window opening measurement by changing the negative reversal potential to higher overpotentials. The features C1' (ca. 1.9 V), C2' (ca. 1.4 V), and A1' (ca. 2.7 V) correspond to processes apparent in the pure ionic liquid as well (see Figure 1), which are not influenced after the addition of sodium, whereas the features C1–C4 and A1–A5 appear in presence of the sodium salt. UPD commences negative of 1.2 V and includes the peaks C1–C3. C1 (ca. 1.15–1.1 V) appears to be the nucleation and C2 (ca. 1.0 V) is the first island formation at those nuclei, as is observed in the in-situ STM measurements (Figure 3b). Further UPD based on the first two processes is observed at a slightly more negative potential at C3 (ca. 0.6 V). It should be noted, that the transferred charge within C3 covers ca. 5.6 mC cm<sup>-2</sup> between 0.9 V and 0.5 V, which would correspond to 25 monolayers of deposit. It can be assumed that part of this charge is related to side reactions. Nevertheless, this is a strong indication of alloy formation, since a typical UPD would stop after deposition of 1–3 layers. Lithium shows a similar behaviour with a rather broad UPD regime that begins at quite high underpotential shifts of 0.5–1.0 V.<sup>[17,23,24]</sup> These literature studies for Li deposition, nonetheless, specify a single broad UPD feature, similar to C3, but not the two additional processes C1 and C2 we could observe for Na deposition (Figure 2). The Na UPD is followed by overpotential deposition (OPD) at C4, *i.e.*, by definition, at potentials below 0 V. A similar OPD feature has been observed for sodium deposition on a layer of sodium-gold alloy,<sup>[31]</sup> but has not been reported for lithium deposition studies.<sup>[17,23,24]</sup> After repeated cycling, reversible dissolution is observed (Figure S2) which indicates that the formed alloy is not completely dissolved during the positive potential excursion. This observation is similar to the deposition and dissolution of sodium on a sodium gold alloy from an organic electrolyte.<sup>[31]</sup> This indicates that during the initial cycles, alloy formation is dominating and pure bulk sodium is absent on the electrode surface at the beginning of the experiment.

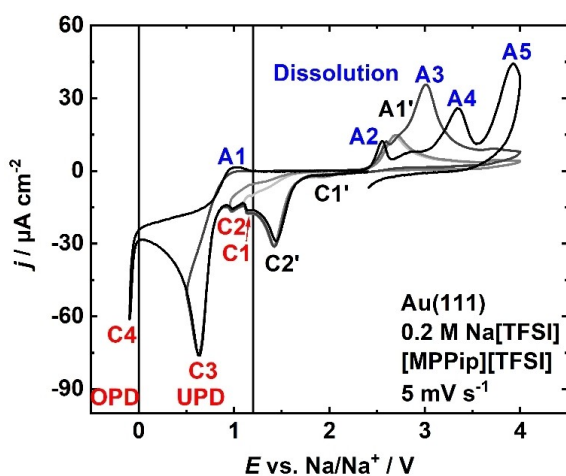


**Figure 2.** Current-potential curves of Au(111) in [MPPip][TFSI] + 0.2 M Na[TFSI] with different negative potential limits. All curves were recorded as consecutive cycles. The black labeled features C1', C2', and A1' are properties of the ionic liquid that are not influenced by the addition of sodium, whereas the red and blue labelled features are attributed to sodium deposition and dissolution, respectively.

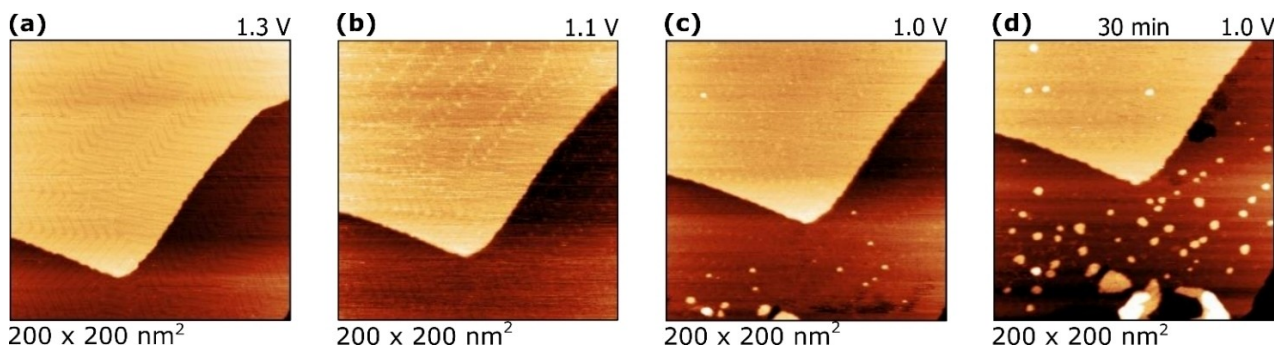


**Figure 3.** In-situ STM images of Au(111) in [MPPip][TFSI] containing 0.2 M Na[TFSI] at 1.3 V vs. Na/Na<sup>+</sup> showing the herringbone structure of the reconstructed surface (a), 1.1 V showing Na nucleation preferentially at the elbows (b), 1.0 V showing island formation at the previously formed nuclei (c), and 1.0 V after 30 min depicting the enhanced island growth (d).

The dissolution peaks A1–A5 (ca. 1.0, 2.5, 3.0, 3.3, and 3.9 V) indicate that the dissolution shows a large hysteresis. Distinct peaks most likely arise as a result of sodium dissolution taking place at different coordination sites of the various alloys. Na<sub>2</sub>Au, NaAu, and NaAu<sub>2</sub> alloys have been reported,<sup>[28]</sup> whereas the Na<sub>2</sub>Au and NaAu<sub>2</sub> alloys were observed in electrochemical studies.<sup>[31]</sup> Dissolution with a similarly large hysteresis has also been reported for lithium deposition on Au(111).<sup>[17,23]</sup> The electrochemical investigation of sodium deposition on Au(111) provides the macroscopic basis for the in-situ STM measurements on the nanoscale as described in the following section.

### In-situ scanning tunneling microscopy

Figure 3a depicts an in-situ STM image of a Au(111) electrode in [MPPip][TFSI] containing 0.2 M Na[TFSI] at 1.3 V. The single crystal was immersed at 2.4 V, followed by a single voltammetric cycle between 1.3 V and 3.0 V. After lifting the thermally induced surface reconstruction the potential-induced reconstruction is formed. The image shows the well-known ( $\sqrt{3} \times 22$ ) reconstructed surface with the herringbone structure, which is stable in this potential region in the presence of the sodium-containing ionic liquid. As the electrode potential is swept to 1.1 V, islands form at the so-called “elbows” of the herringbone reconstructed surface with a height much smaller than that of monoatomically high gold or sodium (Figure 3b). This process corresponds to the feature C1 in the current-potential curves in Figure 2 and is most likely explained by the insertion of sodium atoms into the gold lattice at the elbow sites of the herringbone structure.

As the electrode potential is swept more negatively to 1.0 V, corresponding to the feature C2 in the current-potential curves in Figure 2, islands start to grow on the previously formed nucleation sites forming a row of islands in the in-situ STM image (Figure 3c). The island deposition continues, and 7.5% coverage is reached after 30 min (Figure 3d). It is quite safe to assume that the islands are not formed by lifting the reconstruction for several reasons: (i) the measurements indicate that the islands do not occupy a surplus of 4% of reconstruction atoms and therefore do not grow via Ostwald ripening,<sup>[35,36]</sup> (ii) the herringbone structure remains visible even after the island growth; (iii) the island formation would occur in the pure IL, as well, which is not the case (see Figures S1a and S3). Preferential island formation of a foreign substrate on Au(111) following initial nucleation at reconstruction elbows has been observed for the deposition of metals such as nickel,<sup>[37]</sup> cobalt,<sup>[38,39]</sup> and palladium<sup>[40]</sup> from aqueous electrolytes or under UHV conditions.

A further lowering of the electrode potential results in the growth of more islands. While lateral island growth has been observed, the islands' height does not exceed one monolayer as long as the potential is above 0.6 V. Figure 4a shows the electrode surface at 0.6 V after sweeping the potential down from 0.9 V within 15 min. The imaged area shows a monoatomically high gold step edge between two adjacent terraces on which an island coverage of 0.7% is detected.

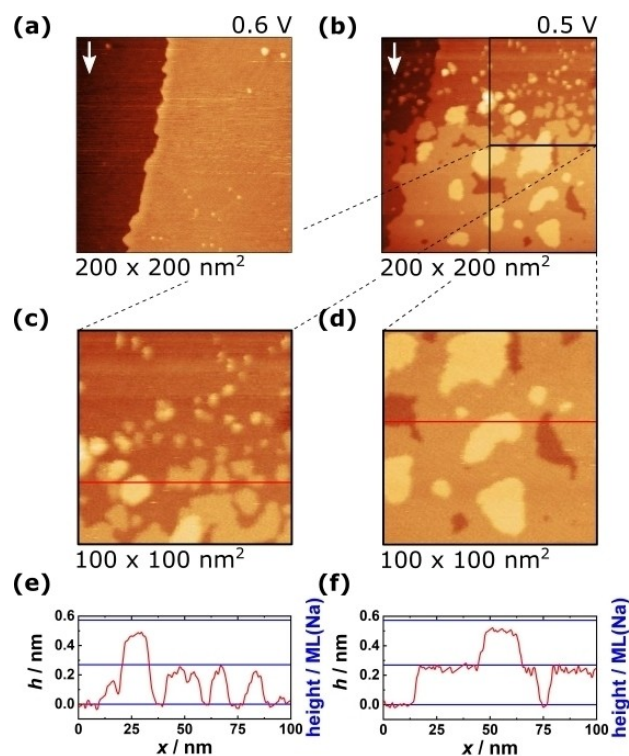


**Figure 4.** In-situ STM image from top to bottom of Au(111) in [MPPip][TFSI] + 0.2 M Na[TFSI] at 0.6 V vs. Na/Na<sup>+</sup> (a) and subsequent image after a potential step to 0.5 V (b), the zoom shots of the bottom and top right area of the STM image in (b). The images were recorded from top to bottom within ca. 10 min (c, d). Corresponding height profiles of the red lines in (c, d), respectively (e, f). The theoretical sodium step height is indicated by the blue horizontal lines.

At 0.5 V (C3 in the current-potential curves in Figure 2), the islands, that have already been formed, grow and coalesce, thus forming layers as depicted in Figure 4b. The in-situ STM image is taken within ca. 10 min beginning after the electrode potential is stepped from 0.6 V to 0.5 V, so in the centre of the image, ca. 5 min have passed after the potential step. It should be noted that the time-stamps are related to the centres of the images. The image is recorded from top to bottom within ca. 10 minutes, revealing the evolution of the structure of the deposit from individual islands into layers. The magnification of Figure 4b (Figure 4c) shows that islands continue forming on the surface in characteristic lines directly after stepping the potential to 0.5 V. In contrast, in the zoom shown in Figure 4d, nearly complete layers have been deposited on the surface. Figures 4e and f show height profiles of the marked lines in Figures 4c and d, respectively. These lines were chosen since they are representative of the change of the deposition within the imaged area from island to layer deposition. The height of 0 nm refers to the gold terrace. The profile in Figure 4e shows several separate islands which cover about 50% of the image and whose heights are around one or two monolayers. In contrast, the height profile in Figure 4f shows that the first monolayer covers about 75% of the image and is only separated into two parts. Hereby, the height profiles are quantified in the order of monolayers. The height information



provides no evidence to distinguish between islands formed of gold (236 pm), sodium (269 pm, for a deposition on gold), or an alloy (height predicted comparable to gold).<sup>[41,42]</sup> There are several reasons for that: i) the height difference is within the instrument's margin of error; ii) co-adsorption of sodium ions may lead to other height values. The coalescence of islands into layers observed in the in-situ STM measurements was previously reported for lithium deposition on Au(111).<sup>[23]</sup> In comparison to the lithium deposition findings, where newly forming lithium islands deposit on previously completed layers, the sodium deposition findings at hand show that newly forming sodium islands are already observed before a previous layer is entirely complete. This could be due to the previously discussed instantaneous formation of a gold-sodium alloy during the very first Na deposition, which constantly alters the surface energy and thus the deposition behaviour. Similar findings in terms of the formation of islands on a previously formed alloy are reported for measurements performed under UHV conditions.<sup>[41]</sup>

The time dependence of Na deposition at 0.5 V is depicted in the in-situ STM images in Figure 5 (scan top to bottom). While imaging at this potential for 40 minutes, the layer growth continues (Figures 5a–d). New layers appear in the image before the underlying layers are completed, up until a point where completion of the layers is no longer reached. Since no further lateral growth is observed (as with layers 3 and 4), the deposition process appears to be kinetically hindered. One reason for the preference for deposition at several surface sites could be the different crystallographic parameters of sodium, gold, and sodium-gold alloys, which cause surface strains and thus prevent smooth layer-by-layer deposition. After 45 minutes of imaging, the morphology of layers changes. More specifically, small nuclei/islands preferably grow near the step edges of the previously deposited layers of sodium (Figures 5d–e). The islands experience three-dimensional growth, forming cauliflower-like structures (Figures 5e–f). According to the observations, the suggested preferred deposition mechanism of sodium on gold is the Stranski–Krastanov mechanism,<sup>[43]</sup> which is known to occur for atoms with radii that very much vary from the atomic radii of the substrate atoms. Interestingly, the growth mode for Li UPD on Au(111) is different,<sup>[17,23,24]</sup> where a three-dimensional growth was observed for Li overpotential deposition (OPD).<sup>[17]</sup>

Figure 6 shows the time dependence of the extracted coverage of each layer to the surface area for the first 40 minutes of deposition (from Figure 4a to Figure 5d). The graph presents that the gold layers are nearly completely covered by sodium or a sodium-gold alloy after five minutes. As soon as layers 4 and 5 cover approximately 50% of the surface, further lateral growth is hindered. This could be explained by several reasons: (i) diffusion of sodium ions through the electrolyte, (ii) diffusion of sodium or gold atoms through the alloy, or (iii) strain caused by the radii difference between sodium and gold atoms which could hinder lateral growth. After 40 minutes (indicated in the graph), layers 6–9 are dominating the surface since they cover more than half of the surface. The subsequent deposition took place in a three-dimensional mechanism rather

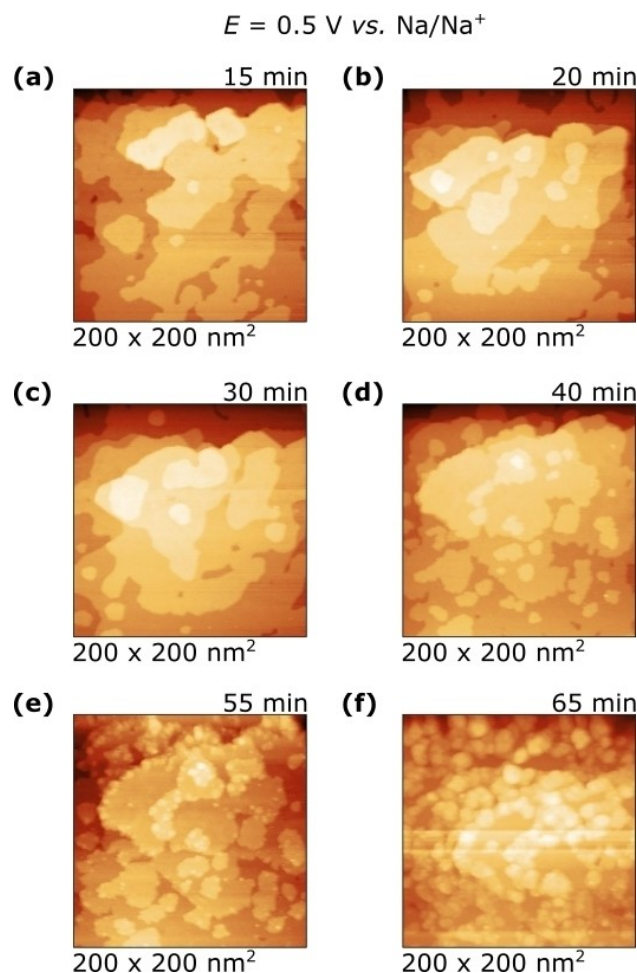


**Figure 5.** In-situ STM images of Au(111) in [MPPip][TFSI] + 0.2 M Na[TFSI] at 0.5 V vs. Na/Na<sup>+</sup> showing further layer growth following Figure 4 after 15 min (a), 20 min (b), 30 min (c) and 40 min (d); as well as a change of the deposition morphology from a layer growth to a 3D-growth after 55 min (e) and the resulting cauliflower-like structure after 65 min (f). The time specifications indicate the growth time at the centre of each STM image after stepping the potential to 0.5 V.

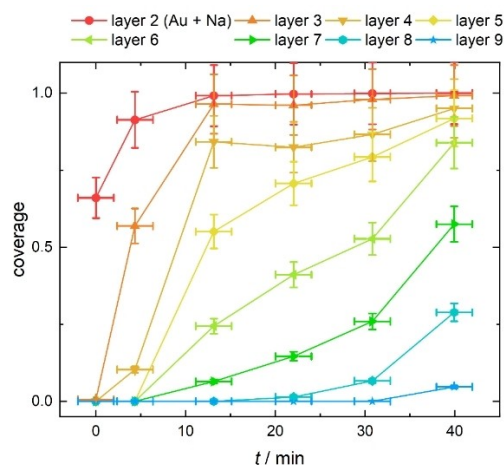


**Figure 6.** Time-dependence of the extracted coverage of each layer for the first 40 minutes of deposition from Figure 4a to Figure 5d.

than layer-by-layer, making further quantification of the deposit very difficult.

The combination of electrochemical and in-situ STM measurements reveals that the Na UPD process follows four subsequent steps: (i) Nucleation of sodium at the so-called elbows of the reconstructed Au(111) surface, followed by (ii) the growth of small monoatomically high islands at the nuclei, which form (iii) a smooth layer by coalescence, and (iv) further islands grow on top of the existing deposited layers where the deposition mode changes from smooth layer formation to three-dimensional growth, resulting in cauliflower-like structures.

The preferential nucleation of sodium at the elbows of the Au(111) surface reconstruction is a very interesting aspect. Although several studies have reported a similar behaviour for other metals,<sup>[37–40,46–58]</sup> a UHV study of sodium deposition on Au(111) has not reported such structures.<sup>[30]</sup> In addition, cobalt shows these structures under UHV and in an aqueous solution.<sup>[38,39]</sup> However, for sodium, the electrolyte seems to play a decisive role.

Another noteworthy result is that the overall UPD process comprises significantly more than two monolayers which is rather unusual given that the nature of the substrate should not exceed two layers of deposition. However, spontaneous alloy formation between sodium and gold is assumed meaning that the deposited layers imaged by in-situ STM consist of a sodium-gold alloy rather than pure sodium. This is supported by several additional facts: (i) Surface alloy formation has been observed for the sodium deposition on Au(111) under UHV conditions already.<sup>[30,41]</sup> (ii) The dissolution of sodium is severely hindered and comprises various features in the current-potential curves. These features might correspond to the dissolution of sodium from different coordination sites with varying binding energies. In addition, different features in the dealloying process from Na<sub>2</sub>Au and NaAu<sub>2</sub> alloys have been reported.<sup>[31]</sup> (iii) After several overpotential deposition and dissolution cycles, reversible processes revealed by the current-potential curves at the Na/Na<sup>+</sup> equilibrium potential can be related to the unhindered sodium deposition and dissolution. This behaviour is very similar to that observed for Na deposition and dissolution on a sodium-gold alloy.<sup>[31]</sup> (iv) Despite the difficulties in observing the dissolution process using in-situ STM, the surface imaged after sodium dissolution appears quite similar to other surfaces after dealloying processes,<sup>[44,45]</sup> indicated by a high density of monoatomic high islands and pits.

Overall, there are numerous similarities to the well-studied Li/Au(111) system. In both cases, the peak-to-peak separation between metal deposition and dissolution is relatively high and an indication of alloy formation. Both alkali metals exhibit an amount much larger than one monolayer deposited in the UPD regions, while the quantity of lithium is smaller compared to sodium.<sup>[17,23]</sup> Other similarities include the coalescence of islands into smooth layers during the UPD<sup>[23]</sup> and three-dimensional deposition, which for lithium takes place in the OPD regime.<sup>[17]</sup>

## Conclusion

The electrochemical behaviour of an Au(111) electrode in a sodium-containing ionic liquid was studied by cyclic voltammetry and in-situ STM. Different initial stages of sodium deposition on gold were observed. The deposition was divided into several stages of UPD and OPD. The UPD began with nucleation and island formation at the elbow sites of the reconstructed Au(111) surface. A similar deposition behaviour was observed for other metals under UHV conditions or with aqueous electrolytes, but so far not with ionic liquids. The formation and growth of islands dominated the deposition behaviour between 1.2 and 0.55 V. A coalescence of the islands into layers could be observed at lower UPD shifts, followed by a three-dimensional growth leading to a cauliflower-like structure, which comprised more than eight monolayers. This rather large amount of UPD indicated spontaneous alloy formation, implying that additional sodium was deposited onto a sodium-gold alloy rather than on previously deposited sodium. The dissolution had a large hysteresis and took place more than 2 V positive of the deposition potential. It could also be broken down into numerous processes, which most likely represented the extraction of sodium from a sodium-gold alloy's differently coordinated sites. In conclusion, these findings pointed out the similarities and differences between the well-known initial stage studies of lithium deposition and the rather unexplored initial stages of sodium deposition. Further in-situ STM measurements were required to study the potential-dependent kinetics of sodium deposition.

## Experimental Section

### Preparation of electrodes and electrolyte

The same Au(111) single crystal (12 mm diameter, MaTeck, Jülich, Germany) was used for all measurements. Before each measurement, the single crystal was thermally annealed in a furnace (Carbolite CWF 1200) at 960 °C for at least 2 h.

The preparation of the sodium reference electrode (RE) was done shortly before the measurement inside a nitrogen-filled glovebox (MBRAUN LABstar, H<sub>2</sub>O, and O<sub>2</sub> ≤ 0.5 ppm) from sodium (≥ 99%, Merck, Darmstadt, Germany) stored in paraffin oil. Subsequently, the outer metal was cut and discarded, taking only the inner part of the sodium to prevent cross-contaminations. From the inner part, a small rod was cut, fixed with a crocodile clip, and aligned with the measuring cell.

The Al/AIPO<sub>4</sub> RE was prepared from an aluminium wire (99.95%, MaTeck). This pseudo reference electrode showed good stability in the system under study and a stable potential at 2 V vs. Na/Na<sup>+</sup>. This potential shift was calculated by the peak potentials of C2', which occurs in measurements with and without the sodium salt.

A loop of a platinum wire was used as a counter electrode.

The ionic liquid [MPPip][TFSI] (99%, IoLiTec, Heilbronn) was dried by heating under a vacuum at 80 °C overnight before usage.

For the sodium-containing electrolyte, Na[TFSI] (99.5%, Solvionic, Toulouse) was added to the pre-dried [MPPip][TFSI] in the glovebox

to form a 0.2 M solution. Afterwards, the solution was dried again by heating under a vacuum at 80 °C overnight.

### Electrochemical measurements

All electrochemical measurements were performed in a nitrogen-filled glovebox (MBRAUN LABstar, H<sub>2</sub>O, and O<sub>2</sub> ≤ 0.5 ppm) using a Zahner IM6 potentiostat and the corresponding software. The electrochemical cell was an in-house designed miniaturised cell set-up similar to the set-up used for in-situ STM measurements. For these measurements, the sodium RE was used. Due to the overlap of different features, the onset potentials of specific processes were estimated by fitting the linear region of the rising part of the peaks and the intersection of this line with the x-axis.<sup>[59]</sup>

### In-situ STM measurements

All in-situ STM measurements were performed with a Veeco MultiMode 8 device with the NanoScope 5 controller and the corresponding Nanoscope Software 8.15. The electrochemical cell was kept under a nitrogen atmosphere using an inert chamber, which was purged with nitrogen before the measurement for at least 10 min and during the addition of the electrolyte. The electrolyte was added under potential control at 2.4 V vs. Na/Na<sup>+</sup>. Before each measurement, a cyclic voltammogram was recorded to control the potential of the Al/AlPO<sub>4</sub> pseudo-RE. Hereby, the potential of the working electrode was varied between 1.5 V and 3 V vs. Na/Na<sup>+</sup>. All images were recorded in the constant-current-mode with tunnelling currents of 0.8–2 nA. All potentials in this study are quoted against the sodium RE. In the STM images, the height increases from dark to bright colour.

The STM tips were produced by etching a Pt/Ir wire (80:20, diameter 0.25 mm, 99.99%, MaTeck, Jülich, Germany) in sodium cyanide solution. Afterwards, the etched tips were coated with molten polyethylene (Lupolen 5031L, LyondellBasell, Rotterdam) to prevent contact between tip and electrolyte.

### Acknowledgements

The authors wish to thank Dr. Maximilian U. Cebelin and Sven J. Zeller for their support in the planning of the measurements and Dr. Maximilian J. Eckl for his additional technical support. This research was funded by the Deutsche Forschungsgemeinschaft (DFG, German Science Foundation) under Germany's Excellence Strategy – EXC 2154 – Project number 390874152 as well as the priority program SPP-2248 – Project number 441209207. Further, support by the BMBF through the InnoSüd-project (Grant Agreement: 03IH5024D) is gratefully acknowledged. Open Access funding enabled and organized by Projekt DEAL.

### Conflict of Interest

The authors declare no conflict of interest.

### Data Availability Statement

The data that support the findings of this study are available in the supplementary material of this article.

**Keywords:** alloy formation · electrodeposition · ionic liquids · post-lithium batteries · scanning probe microscopy

- [1] G. A. Giffin, *J. Mater. Chem. A* **2016**, *4*, 13378–13389.
- [2] B. L. Ellis, L. F. Nazar, *Curr. Opin. Solid State Mater. Sci.* **2012**, *16*, 168–177.
- [3] M. Wang, F. Zhang, C.-S. Lee, Y. Tang, *Adv. Energy Mater.* **2017**, *7*, 1700536.
- [4] M. S. Islam, C. A. J. Fisher, *Chem. Soc. Rev.* **2014**, *43*, 185–204.
- [5] P. Adelhelm, P. Hartmann, C. L. Bender, M. Busche, C. Eufinger, J. Janek, *Beilstein J. Nanotechnol.* **2015**, *6*, 1016–1055.
- [6] R. Wibowo, L. Aldous, E. I. Rogers, S. E. Ward Jones, R. G. Compton, *J. Phys. Chem. C* **2010**, *114*, 3618–3626.
- [7] B. Lee, E. Paek, D. Mitlin, S. W. Lee, *Chem. Rev.* **2019**, *119*, 5416–5460.
- [8] Y. Yui, M. Hayashi, J. Nakamura, *Sci. Rep.* **2016**, *6*, 22406.
- [9] K. Matsumoto, T. Hosokawa, T. Nohira, R. Hagiwara, A. Fukunaga, K. Numata, E. Itani, S. Sakai, K. Nitta, S. Inazawa, *J. Power Sources* **2014**, *265*, 36–39.
- [10] K. Pfeifer, S. Arnold, J. Becherer, C. Das, J. Maibach, H. Ehrenberg, S. Dsoke, *ChemSusChem* **2019**, *12*, 3312–3319.
- [11] P. Verma, P. Maire, P. Novák, *Electrochim. Acta* **2010**, *55*, 6332–6341.
- [12] L. S. Plashnitsa, E. Kobayashi, Y. Noguchi, S. Okada, J. Yamaki, *J. Electrochem. Soc.* **2010**, *157*, A536–A543.
- [13] F. Endres, S. Zein El Abedin, *Phys. Chem. Chem. Phys.* **2006**, *8*, 2101–2116.
- [14] R. Hayes, G. G. Warr, R. Atkin, *Chem. Rev.* **2015**, *115*, 6357–6426.
- [15] S. A. Mohd Noor, P. C. Howlett, D. R. MacFarlane, M. Forsyth, *Electrochim. Acta* **2013**, *114*, 766–771.
- [16] T. Pajkossy, C. Müller, T. Jacob, *Phys. Chem. Chem. Phys.* **2018**, *20*, 21241–21250.
- [17] C. A. Berger, M. U. Cebelin, T. Jacob, *ChemElectroChem* **2017**, *4*, 261–265.
- [18] F. M. Schuett, M. Heubach, J. Mayer, M. U. Cebelin, L. A. Kibler, T. Jacob, *Angew. Chem. Int. Ed.* **2021**, *60*, 20461–20468.
- [19] D. M. Kolb, *Angew. Chem.* **2001**, *113*, 1198–1220; *Angew. Chem. Int. Ed.* **2001**, *40*, 1162–1181.
- [20] E. Herrero, L. J. Buller, H. D. Abruña, *Chem. Rev.* **2001**, *101*, 1897–1930.
- [21] M. Dietterle, T. Will, D. M. Kolb, *Surf. Sci.* **1995**, *342*, 29–37.
- [22] M. A. Schneeweiss, D. Kolb, *Chem. Unserer Zeit* **2000**, *34*, 72–83.
- [23] L. H. S. Gasparotto, N. Borisenko, N. Bocchi, S. Zein El Abedin, F. Endres, *Phys. Chem. Chem. Phys.* **2009**, *11*, 11140–11145.
- [24] X. Hu, C. Chen, S. Tang, W. Wang, J. Yan, B. Mao, *Sci. Bull.* **2015**, *60*, 877–883.
- [25] K. M. Schüttler, J. Bansmann, A. K. Engstfeld, R. J. Behm, *J. Chem. Phys.* **2020**, *152*, 124701.
- [26] M. J. Esplandiu, M. A. Schneeweiss, D. M. Kolb, *Phys. Chem. Chem. Phys.* **1999**, *1*, 4847–4854.
- [27] M. H. Hölzle, U. Retter, D. M. Kolb, *J. Electroanal. Chem.* **1994**, *371*, 101–109.
- [28] A. D. Pelton, *Bull. Alloy Phase Diagrams* **1986**, *7*, 136–139.
- [29] S. Tang, Z. Qiu, X. Y. Wang, Y. Gu, X. G. Zhang, W. W. Wang, J. W. Yan, M. Sen Zheng, Q. F. Dong, B. W. Mao, *Nano Energy* **2018**, *48*, 101–106.
- [30] J. V. V. Barth, H. Brune, R. Schuster, G. Ertl, R. J. J. Behm, *Surf. Sci.* **1993**, *292*, L769–L774.
- [31] S. Tang, Y. Y. Zhang, X. G. Zhang, J. T. Li, X. Y. Wang, J. W. Yan, D. Y. Wu, M. Sen Zheng, Q. F. Dong, B. W. Mao, *Adv. Mater.* **2019**, *31*, 1–7.
- [32] M. Han, C. Zhu, T. Ma, Z. Pan, Z. Tao, J. Chen, *Chem. Commun.* **2018**, *54*, 2381–2384.
- [33] L. Geng, Q. Liu, J. Chen, P. Jia, H. Ye, J. Yan, L. Zhang, Y. Tang, J. Huang, *Nano Res.* **2022**, *15*, 2650–2654.
- [34] A. I. Yanson, P. Rodriguez, N. Garcia-Araez, R. V. Mom, F. D. Tichelaar, M. T. M. Koper, *Angew. Chem. Int. Ed.* **2011**, *50*, 6346–6350; *Angew. Chem.* **2011**, *123*, 6470–6474.
- [35] N. J. Tao, S. M. Lindsay, *J. Appl. Phys.* **1991**, *70*, 5141–5143.
- [36] D. M. Kolb, *Prog. Surf. Sci.* **1996**, *51*, 109–173.
- [37] D. D. Chambliss, R. J. Wilson, S. Chiang, *Phys. Rev. Lett.* **1991**, *66*, 1721–1724.

- [38] B. Voigtländer, G. Meyer, N. M. Amer, *Phys. Rev. B* **1991**, *44*, 10354–10357.
- [39] M. Kleinert, H. F. Waibel, G. E. Engelman, H. Martin, D. M. Kolb, *Electrochim. Acta* **2001**, *46*, 3129–3136.
- [40] A. W. Stephenson, C. J. Baddeley, M. S. Tikhov, R. M. Lambert, *Surf. Sci.* **1998**, *398*, 172–183.
- [41] J. V. Barth, R. J. Behm, G. Ertl, *Surf. Sci.* **1995**, *341*, 62–91.
- [42] E. J. Kwolok, R. Widmer, O. Gröning, O. Deniz, H. Walen, C. D. Yuen, W. Huang, D. L. Schlagel, M. Wallingford, P. A. Thiel, *Inorg. Chem.* **2015**, *54*, 1159–1164.
- [43] I. N. Stranski, L. Krastanow, *Monatsh. Chem.* **1937**, *71*, 351–364.
- [44] M. C. del Barrio, S. G. García, D. R. Salinas, *Electrochem. Commun.* **2004**, *6*, 762–766.
- [45] J. Erlebacher, K. Sieradzki, *Scr. Mater.* **2003**, *49*, 991–996.
- [46] S. Padovani, F. Scheurer, J. P. Bucher, *Europhys. Lett.* **1999**, *45*, 327–333.
- [47] K. Schouteden, E. Lijnen, E. Janssens, A. Ceulemans, L. F. Chibotaru, P. Lievens, C. Van Haesendonck, *New J. Phys.* **2008**, *10*, 043016.
- [48] H. Takeshita, Y. Suzuki, H. Akinaga, W. Mizutani, K. Ando, T. Katayama, A. Itoh, K. Tanaka, *J. Magn. Magn. Mater.* **1997**, *169*, 38–41.
- [49] C. Tölkes, P. Zeppenfeld, M. A. Krzyzowski, R. David, G. Comsa, *Phys. Rev. B: Condens. Matter Mater. Phys.* **1997**, *55*, 13932–13937.
- [50] J. Wollschläger, N. M. Amer, *Surf. Sci.* **1992**, *277*, 1–7.
- [51] E. I. Altman, R. J. Colton, *Surf. Sci.* **1994**, *304*, L400–L406.
- [52] M. M. Biener, J. Biener, R. Schalek, C. M. Friend, *Surf. Sci.* **2005**, *594*, 221–230.
- [53] C. S. Casari, S. Foglio, F. Siviero, A. Li Bassi, M. Passoni, C. E. Bottani, *Phys. Rev. B: Condens. Matter Mater. Phys.* **2009**, *79*, 1–25.
- [54] J. A. Meyer, I. D. Baikie, E. Kopatzki, R. J. Behm, *Surf. Sci.* **1996**, *365*, 647–651.
- [55] F. A. Möller, O. M. Magnussen, R. J. Behm, *Phys. Rev. Lett.* **1996**, *77*, 5249–5252.
- [56] I. Chado, C. Goyhenex, H. Bulou, J. P. Bucher, *Appl. Surf. Sci.* **2004**, *226*, 178–184.
- [57] L. Cagnon, A. Gundel, T. Devolder, A. Morrone, C. Chappert, J. E. Schmidt, P. Allongue, *Appl. Surf. Sci.* **2000**, *164*, 22–28.
- [58] T. H. Gentner, F. Scheurer, T. Detzel, J. P. Bucher, *Thin Solid Films* **1996**, *275*, 58–60.
- [59] S. Z. El Abedin, F. Endres, *Electrodeposition from Ionic Liquids*, Wiley-VCH Verlag GmbH & Co. KGaA, Weinheim, Germany, **2017**.

Manuscript received: June 30, 2022

Revised manuscript received: July 26, 2022

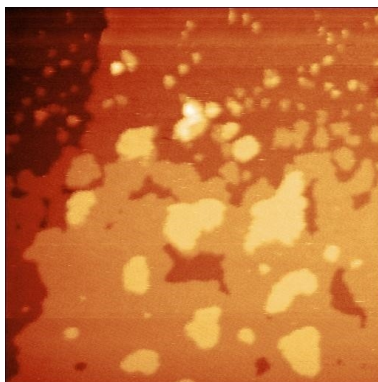
Accepted manuscript online: July 27, 2022



## RESEARCH ARTICLE

---

**In-situ deposition study:** Sodium was deposited onto Au(111) from an ionic liquid. It revealed a rather extensive underpotential deposition, which took place in four different stages. The complete process from initial nucleation on the elbows of the herringbone reconstruction to the formation of a cauliflower-like structure was observed by in-situ STM.



*M.-K. Heubach, F. M. Schuett, Dr. L. A. Kibler, Dr. A. Abdelrahman\*, Prof. Dr. T. Jacob\**

1 – 9

**Initial Stages of Sodium Deposition onto Au(111) from [MPPip][TFSI]: An In-Situ STM Study for Sodium-Ion Battery Electrolytes**



Open Access